Langmuir

Article

pubs.acs.org/Langmuir

Colloidal Crystallization and Structural Changes in Suspensions of Silica/Magnetite Core−Shell Nanoparticles

Vikash Malik,*[,†] Andrei V. Petukhov,[‡] Le He,[§] Yadong Yin,[§] and Marius Schmidt[†]

[†]Physics Department, University of Wisconsin—Milwaukee, 1900 E. Kenwood Blvd., Milwaukee, Wisconsin 53211, United States

[‡]van 't Hoff Laboratory for Physical and Colloid Chemistry, Debye Institute for Nanomaterials Science, Utrecht University, The Netherlands

[§]Department of Chemistry, University of California—Riverside, 501 Big Springs Road, Riverside, California 92521, United States

ABSTRACT: The microradian X-ray scattering technique is used to investigate the colloidal crystallization of silica/magnetite core−shell magnetic nanoparticles. Particle self-assembly ranging from 2D sheets to 3D semicrystalline structures is observed as a function of the sedimentation-induced variation of the local particle concentration and the applied magnetic field. Because the particle size is comparable to the wavelength of light, these structures possess photonic properties that can be manipulated by an external stimulus.

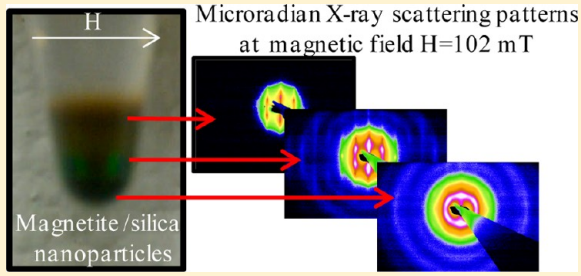

INTRODUCTION

Magnetic nanoparticles have unique colloidal, magnetic, and optical properties that differ from their bulk counterparts.[1,2] Dipolar interactions between colloidal particles can lead to a plethora of novel phases ranging from string fluids to crystalline phases with unusual symmetries.[3−8] Core−shell nanoparticles have been a topic of great interest because of their potential use in biology,[9,10] imaging,[11] medicine,[12−14] and DNA separation.[15,16] Colloidal suspensions of magnetic nanoparticles can self-assemble into ordered structures. The ability to manipulate this assembly by external tuning parameters such as field, temperature, and concentration is essential to develop new stimuli-responsive materials.

In 2007, the Yin group synthesized novel superparamagnetic magnetite colloidal nanoparticles that can self-assemble into 1D particle chains and exhibit excellent tunable photonic properties.[17] A suspension of these nanoparticles displays tunable colors in the visible range of the electromagnetic spectrum. The freedom to tune the diffraction color not only depends on the particle size but also varies with the strength of an applied external magnetic field. Since then, there has been widespread interest in these nanoparticles and their applications. For example, Ge et al. reported that silica-covered magnetite core−shell nanoparticles can be used to fabricate humidity sensors and photonic papers.[18,19] Very recently, He et al. demonstrated the modulation of the local assembly of superparamagnetic nanoparticles that results in the creation of novel color patterns.[20]

Despite their tremendous potential in various applications, interesting fundamental questions that refer to their colloidal crystallization with and without the magnetic field remain unanswered. For example, in a recent study, He et al. suggested that it is possible to induce a phase transition from 1D particle chains to 3D colloidal crystals by manipulating the magnetic field in photonic structures.[21] The chainlike 1D photonic structures form in a weak magnetic field and exhibit a fast, reversible response to external magnetic fields. Increasing the strength and gradient of the magnetic field induces the evolution from 1D chains to 2D sheets, which results eventually in 3D structures. It is suspected that the phase transition is related to an increase in the local concentration of the magnetic particles when they are exposed to magnetic fields over a relatively long period of time. However, detailed in situ studies of how the crystalline phase varies with the strength of the magnetic field and with the concentration of the magnetic particles are not available. In this article, we use the microradian X-ray scattering technique to probe the assembly and phase behavior of a magnetic colloidal suspension using a concentration gradient created by sedimentation. We show that the colloidal crystallization of silica/magnetite nanostructures not only depends on the strength of the external magnetic fields but also varies with the local concentration in the sediment of these nanoparticles.

MATERIAL AND METHODS

Materials. Anhydrous iron(III) chloride ($FeCl_3$), sodium hydroxide (NaOH), ammonium hydroxide solution (27% in H_2O), tetraethyl orthosilicate (TEOS), and ethanol were purchased from Fisher Scientific. Polyacrylic acid (PAA, MW = 1800) and diethylene glycol (DEG) were obtained from Sigma-Aldrich. Distilled water was used in all experiments. All chemicals were used without further treatment and/or purification.

Synthesis of Silica/Magnetite. For the synthesis of Fe_3O_4 nanoclusters, 4 mmol of PAA and 0.4 mmol of $FeCl_3$ are dissolved in 17 mL of DEG. This solution was heated to 220 °C under a

Received: May 11, 2012
Revised: July 12, 2012
Published: July 13, 2012

 © 2012 American Chemical Society dx.doi.org/10.1021/la301942t | Langmuir 2012, 28, 14777−14783

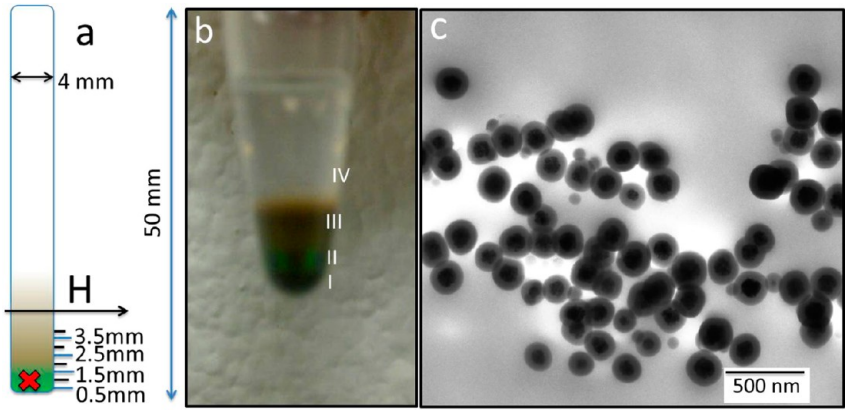

Figure 1. (a) Scheme of a test capillary used for data collection during the experiment. Red cross perpendicular to the long axis of the capillary: direction of incident beam. Black arrow: direction of the magnetic field. Positions along the capillary axis are marked. (b) Image of an Eppendorf tube containing a suspension of silica/magnetite core–shell nanoparticles in ethanol. Positions I–III: sediment. Position IV: ethanol. (c) Transmission electron microscopy (TEM) image of silica/magnetite core–shell nanoparticles.

nitrogen atmosphere for 1 h, after which it became transparent. Then, 1.75 mL of a NaOH/DEG mixture (2.5 mol/L) was injected. The mixture was heated for an additional hour at 220 °C. The black color of the solution confirms the formation of magnetite nanoclusters. This solution is then cooled to room temperature and repetitively cleaned with a mixture of water and ethanol. For the silica layer coating, the Fe_3O_4 nanoclusters were dispersed in 3 mL of water and mixed with 1 mL of ammonium hydroxide (27% in H_2O) and 20 mL of ethanol. After 20 min of stirring, 200 μL of TEOS was injected into the solution. Stirring was stopped 40 min after the injection. The suspension of Fe_3O_4@SiO_2 particles was cleaned three times with ethanol and finally dispersed in 1 mL of ethanol.[22]

Characterization. The morphology of the Fe_3O_4@SiO_2 colloid was characterized using a Hitachi (HAR-60) transmission electron microscope (TEM). Scattering experiments with hard X-rays (λ = 1 Å) were performed at Dutch–Belgian beamline BM-26B of the European Synchrotron Radiation Facility (ESRF) in Grenoble, France,[23] where a microradian X-ray diffraction setup[24,25] was used. A magnetic field perpendicular to the X-ray beam was generated by a variable-field permanent magnet kindly provided by the ID-02 beamline. In investigating the colloidal structure formation, several rectangular capillaries were filled with a suspension of core–shell nanoparticles. The particles were allowed to sediment freely under gravity for 24 h, and then the vertical z position was marked as shown in the scheme in Figure 1a. A magnetic field of variable strength was applied perpendicular to the vertical axis of the capillary as indicated by the black arrow in Figure 1a. The direction of the X-ray beam was always perpendicular to the direction of the external magnetic field as indicated by a cross (Figure 1a). Scattering patterns were observed at different z positions, from z = 0.5 to 3.5 mm, measured from the bottom of the capillary. The magnetic fields used in this study were 48, 102, and 223 mT. For the position-dependent measurements, the magnetic field was kept fixed at its respective value and the position of the sample was changed by moving the capillary downward or upward.

Model to Explain the Experimental Results. The positional and magnetic field dependence of the colloidal assembly of silica/magnetite nanoparticles arises from a sensitive interplay among the local concentration of the particles in the capillary, the effect of the thermal energy, and three types of forces between the colloidal nanoparticles. These are (1) the hard-sphere repulsion between particles at contact; (2) a combination of electrostatic repulsion due to the presence of charges on the surfaces of nanoparticles and van der Waals attraction; and (3) magnetic dipolar attraction/repulsion due to the magnetite core of the particles. The interaction potential of the later is given by

$$U_{ab}(r) = \frac{1}{r^3}(\vec{\mu}_a \cdot \vec{\mu}_b) - \frac{3}{r^5}(\vec{\mu}_a \cdot \vec{r}_{ab})(\vec{\mu}_b \cdot \vec{r}_{ab}) \quad (1)$$

The dipolar interaction between two magnetic particles a and b depends on the magnitude and direction of their magnetic moments μ_a, μ_b, respectively, and their relative position r_{ab}. Depending on the particles' configuration, the dipolar energy term may be repulsive or attractive. Heinrich and co-workers showed that these forces play a role in the assembly of magnetic nanoparticles.[26] When a magnetic field is applied, these particles initially form chainlike structures. These chains then arrange into 2D hexagonally packed sheets. This occurs by shifting a neighboring chain by a distance r corresponding to the radius of the nanoparticles. In Figure 2a, a hexagonally packed sheet of particles is shown. Each sheet is made of chains of nanoparticles. The chains are formed along the direction of an external magnetic field

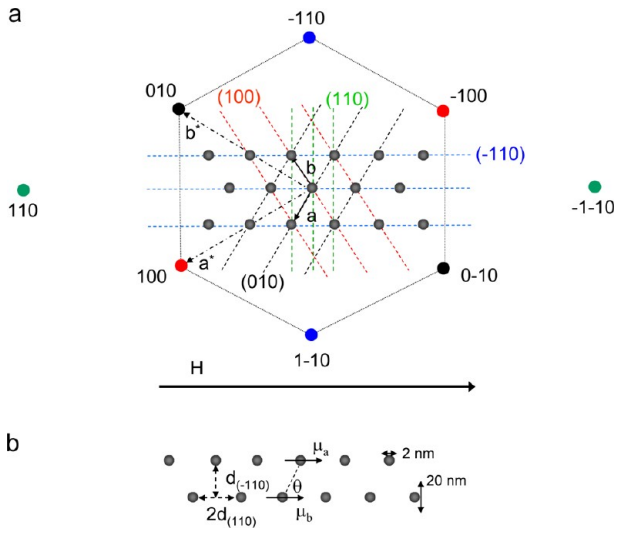

Figure 2. Schematic representation of a hexagonal sheet made of nanoparticles (gray spheres). (a) Black arrows: real space unit cell vectors a and b. Planes (dashed lines) are shown with Miller indices in parentheses: red, (100) planes; black, (010) planes; green, (110) planes; and blue, (−110) planes. Dashed–dotted arrows: reciprocal space unit vectors a* and b*. Reflections and their corresponding planes are shown in the same color. Reflections are also marked by their respective indices. The dotted hexagon outlines the hexagonal symmetry of the reflection pattern. The direction of the magnetic field H is also shown. (b) Relevant distances d between the chains and particles, the angle θ between magnetic moments and the line connecting them, and the range of distance changes observed in the diffraction pattern are shown.

dx.doi.org/10.1021/la301942t | *Langmuir* 2012, 28, 14777–14783

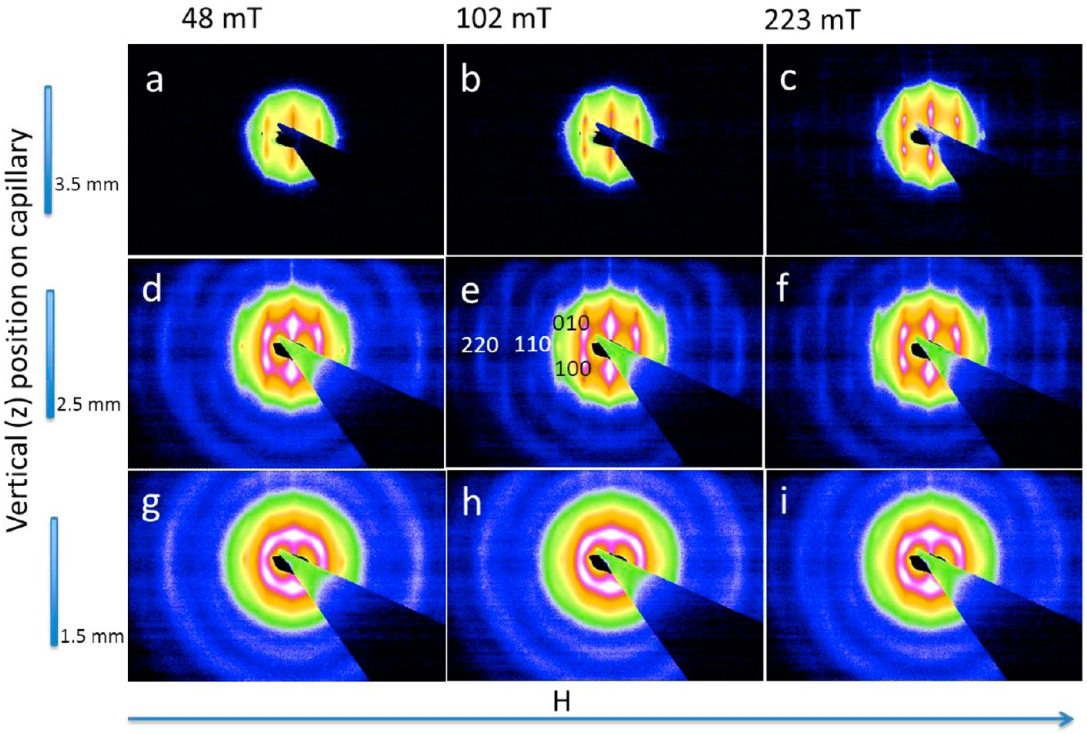

Figure 3. Scattering patterns obtained at different z positions as shown in the schematic on the left-hand side of the image and at different magnetic fields H, as shown at the top of this image. z = 3.5 mm: (a) 48, (b) 102, and (c) 223 mT. z = 2.5 mm: (d) 48, (e) 102, and (f) 223 mT. z = 1.5 mm: (g) 48, (h) 102, and (i) 223 mT. The reflection indices are shown in scattering pattern e. The direction of the magnetic field is also shown (arrow).

(H). The relevant lattice planes are also shown. The scattering of X-rays from the lattice will result in a hexagonal reflection pattern that is sensitive to distances and disorder in the lattice. Bragg reflections perpendicular to the external magnetic field (H) contain information about the distances between the chains in a plane. However, horizontal reflections, which are parallel to the magnetic field, are sensitive to the distances between particles within a chain. Different orientations of the planes around the magnetic field direction give rise to broad peaks in the vertical direction of the diffraction pattern. In contrast, disorder along the chains, intrachain disorder, or chain wobbling will result in weaker horizontal Bragg peaks whose intensity is reduced by a Debye–Waller factor.

RESULTS AND DISCUSSION

Figure 1b shows an Eppendorf tube where silica/magnetite core–shell nanoparticles were allowed to sediment under gravity. Phase separation of the nanoparticles and solvent occurs rapidly. This creates a concentration gradient in the lower part of the tube. The brown color of the colloidal suspension results from the silica-coated magnetite nanoparticles, whereas the green color at the bottom of the tube is a result of the colloidal assembly of these core–shell nanoentities. A TEM image of these nanoparticles is also shown in Figure 1c. The core–shell structure of the nanoparticles becomes apparent. Magnetic field- and concentration-dependent in situ microradian X-ray scattering results in the dispersions of these core–shell particles are shown in the following text.

Upper Part of the Capillary. To investigate the position-dependent crystallization of the core–shell nanostructures, the sediment was scanned at different z positions. At each z position, three scattering patterns corresponding to three different magnetic fields were obtained. Figure 3 shows nine scattering patterns corresponding to z = 3.5, 2.5, and 1.5 mm. All of the nanoparticles are made of same magnetic material,

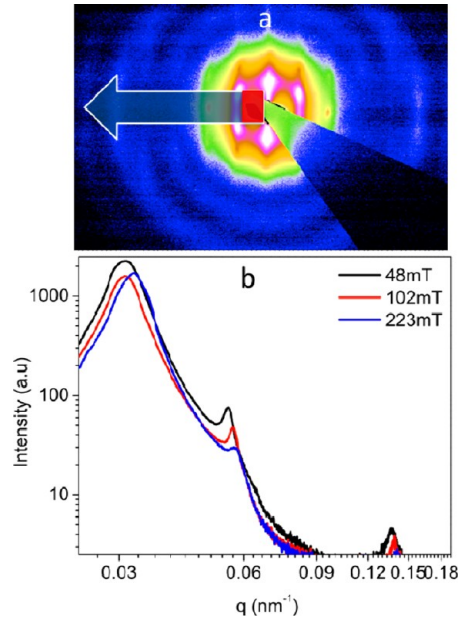

Figure 4. (a) Scattering pattern obtained at z = 2.5 mm and 48 mT. Arrow: section of the pattern that has been used for the intensity integration. Red rectangle: mask area for the beam stop. (b) Intensity vs q curves at z = 2.5 for 48 (black line), 102 (red line) and 223 mT (blue line).

and their size is quite monodisperse. Consequently, the magnetic moment for all of the particles is the same at a given magnetic field H. However, the distance between them will depend on the local concentration.

At vertical position z = 3.5 mm, the suspension of nanoparticles behaves as a normal colloidal system. Once a

dx.doi.org/10.1021/la301942t | Langmuir 2012, 28, 14777–14783

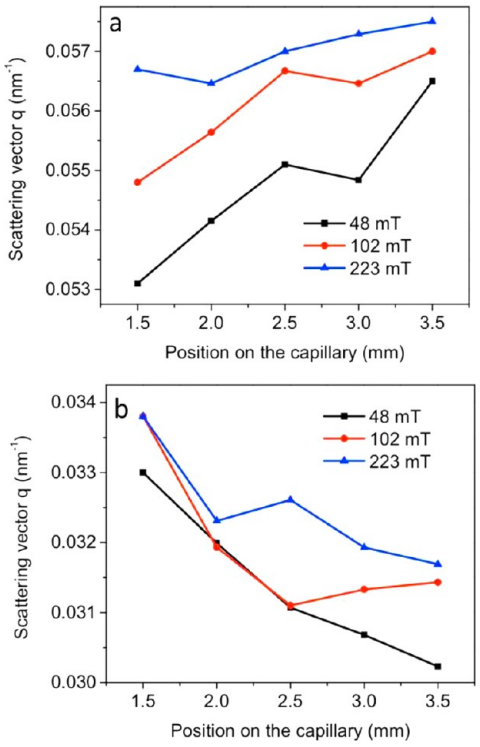

Figure 5. (a) Positions q of the (110) reflection plotted as a function of the vertical z position at 48 (black squares), 102 (red circles), and 223 mT (blue triangles). Lines are guides to the eyes. (b) Positions q of the (100) and (010) reflections plotted as a function of the vertical z position at 48 (black squares), 102 (red circles), and 223 mT (blue triangles). Lines are guides to the eyes.

small magnetic field such as 48 mT is applied, all of the nanoparticles acquire a net magnetic moment in the direction of the magnetic field and align themselves along this direction and form chainlike structures (Figure 3a). The signature of such an assembly is that vertical stripes appear in the X-ray diffraction pattern. The distances between the stripes are inversely proportional to the particle distances in the chains. Note, however, the modulation of the scattering intensity along these vertical stripes, which suggests the presence of positional correlations between neighboring chains. These correlations become much more pronounced upon increasing the magnetic field. A gradual increase in the intensity of the hexagonally ordered features in the scattering pattern (Figure 3b,c) points to the formation of hexagonal sheets. In addition, the ordering of the particle chains increases as witnessed by the appearance of the horizontal (110) reflection. The increase in the chain order in turn also favors the formation of the sheets as shown by the increase in the (010) and (−110) reflection intensities.

At z = 2.5 mm, the local concentration of the particles is higher. The scattering pattern at a weaker field of 48 mT displays a mixture of rings and diffraction spots (Figure 3d). The rings are caused by the form factor of the spherical particles in the sediment. The six diffraction spots at the lowest q values are arranged in the form of a slightly distorted hexagon. The q values for the two reflections (−110) and (1-10) above and below the direct beam are smaller compared to the one of the (110) reflections. This shows that the distances between the chains are larger than those between the particles within a chain. Obviously, the interchain interactions are smaller than the intrachain, interparticle interactions. With increasing

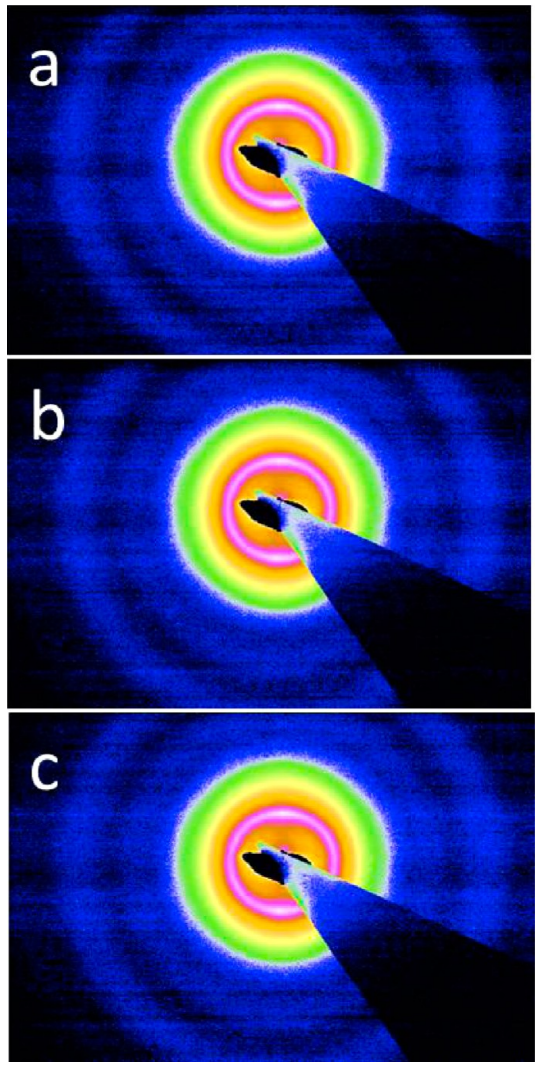

Figure 6. Microradian X-ray scattering patterns obtained at z = 0.5 mm on the capillary at various magnetic fields: (a) 48, (b) 102, and (c) 223 mT.

magnetic field, the outer rings in the scattering patterns become stronger and change to elongated diffraction spots (Figure 3e,f). This leads to the formation of even more hexagonal sheets. We radially averaged the intensity of the diffraction pattern in an area denoted by the arrow in Figure 4a by using Fit2D software (downloaded from the Web site of the European Synchrotron Radiation Facility (ESRF), Grenoble, France). The pixels present in the rectangular arrow have been considered for radial averaging. The radially averaged intensity is plotted as a function of q. Two pronounced peaks appear at two different q values, q_1 and q_2 (Figure 4b). The peak at q_1 results from blurred (010) and (100) reflections, and the peak at q_2 arises from the (110) reflection intensity. The ratio of q_2 to q_1 is 1.80. This value is close to the expected value, 1.73, for a hexagonally packed crystal structure. This confirms that the nanoparticles assemble themselves into a 2D hexagonal crystal structure similar to that for superparamagnetic nanoparticles as observed by others.[27] Compared to z = 3.5, the particle concentration is higher at z = 2.5. This increase will eventually lead to the dominance of interparticle forces, in particular, the magnetic dipole interaction and the van der Waals attraction.

dx.doi.org/10.1021/la301942t | *Langmuir* 2012, 28, 14777−14783

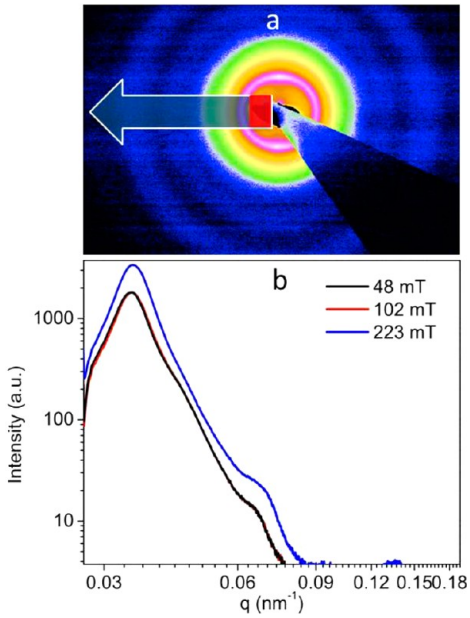

Figure 7. (a) Scattering pattern obtained for z = 0.5 mm and H = 48 mT. Arrow: section of the pattern that has been used for the integration of the intensity. Red rectangle: mask area for the beam stop. (b) Intensity vs q curves at z = 0.5 mm for 48 (black line), 102 (red line), and 223 mT (blue line).

The presence of these two forces facilitates the formation of the hexagonal sheets.

Upon moving further down in the capillary (at z = 1.5 mm), the diffraction rings become relatively compact and the diffraction spots at lower q also fuse together to form a ring while maintaining the hexagonal symmetry (Figure 3g,i). The presence of diffuse rings also gives some evidence for the formation of a disordered structure. Note that the vertical stripes in the X-ray scattering pattern, which were very evident in Figure 2a–f, have nearly disappeared at a high concentration of nanoparticles at z = 1.5 mm. Instead, the scattering occurs along the rings. This is characteristic of a transition from the 2D sheetlike assembly to 3D close-packed structures as also reported earlier by Goyal et al.[28] At the larger particle concentration, the excluded volume interactions start to play an increasingly larger role so that the system is forced to form close-packed 3D structures.

To summarize, the scattering patterns show that the structure formation of the nanoparticles depends on the position in the sediment. In the upper part of the sediment, one can observe the gradual formation of 2D sheetlike structures, which become better ordered upon increasing the magnetic field. The intermediate section (z = 2.5 mm) forms a 2D hexagonal colloidal crystal at both lower and higher magnetic fields. At the bottom of the capillary, a 3D disordered structure appears.

Interplay between Particles and Chains: Bragg Reflections 110, 100, and 010. Figure 5a shows the intensity of the diffraction pattern radially averaged as described above at z = 2.5 mm. The peak at higher q values corresponds to the (110) reflection. As shown in Figure 2, the (110) reflection senses mainly the particle-to-particle distances in a chain. The q value of the (110) reflection increases slightly if the applied magnetic field increases (Figure 5a). At low particle concentration and at small magnetic fields, the particles possess small but sufficient magnetic moments that they can interact to form loosely bound chains. At a higher particle concentration around z = 1.5 mm, van der Waals forces add to the attraction. The particle chain becomes more compact with slightly smaller interparticle distances. At higher magnetic fields such as 103 and 223 mT, the particles possess larger magnetic moments and attract each other even more because of increasingly larger van der Waals and dipolar attraction. However, the distance changes remain small, on the order of 2 nm (Figure 2b). The scattering intensity of the (110) reflection decreases significantly at higher magnetic fields (Figure 3e). The (110) reflection intensity is a measure of the intrachain order. At higher magnetic fields, the very compact chains start to wobble and deviate from the hexagonal symmetry. This disorder also decisively determines the distances between the chains in the hexagonal sheets.

The (100) and (010) reflections are sensitive to chain-to-chain distances in the hexagonal plane (Figure 2). The (100) and (010) reflection positions also display a concentration and magnetic field dependence (Figure 5b). Within the hexagonal geometry, the horizontal and vertical distances observed through the (110) and (010) reflection positions, respectively, give the angle between the dipole moments of particles of adjacent chains. This angle between two magnetic dipoles varies between 53 and 57° (Figure 2b). In this configuration, the dipolar interactions between the chains vanish (eq 1) and the effect of the magnetic field on these reflections should be small. This is indeed observed (Figure 5b). The attractive van der Waals forces also play a role in the formation of hexagonal sheets as reported earlier.[26] As we move down in the capillary, the concentration increases. At a given magnetic field such as 48 mT, the distance corresponding to the (100) or the (010) plane decreases from 210 nm at z = 3.5 mm to 190 nm at z = 1.5 mm. (See also Figure 1b.) This decrease is almost independent of the magnitude of the magnetic field. The vertical reflection positions mainly depend on the concentration of the particles.

Lower Part of the Capillary. Three scattering patterns corresponding to three different values of the magnetic field were recorded at z = 0.5 mm (Figure 6a–c). In all of the scattering patterns, we observe diffraction rings at low as well as high q values.

At higher q values, the rings are somewhat broadened. The intensity of the rectangular section was radially averaged (Figure 7a) and plotted as a function of q to retrieve information about the colloidal assembly. The integrated intensity versus q curves at magnetic fields of 48 and 102 mT overlap with each other, and we observe one pronounced peak at q = 0.036 nm^{-1} (Figure 7b). The position of this peak corresponds to a distance of 190 nm. As determined from the TEM images, the average size of our core–shell nanostructures is 200 ± 25 nm. Therefore, this distance matches the center-to-center distance between two nanoparticles very well if they are arranged in a chain. Furthermore, the peak at q = 0.065 nm^{-1} observed at 48 and 102 mT corresponds to just half of the particle distance. When the magnetic field increases further to 223 mT, both peak intensities increase and the peak maxima shift slightly to higher q values. As observed at lower concentrations, the assembly becomes more compact at higher fields, but no hexagonal symmetry is observed. Recent theoretical work on dipolar colloidal nanoparticles shows that at higher particle concentration long chains of magnetic nanoparticles might entangle to form a disordered struc-

dx.doi.org/10.1021/la301942t | Langmuir 2012, 28, 14777–14783

ture.[29,30] Our observations are in close agreement with these results.

CONCLUSIONS

The scattering patterns reveal 2D hexagonal structures formed by the chains of nanoparticles. This assembly further changes to a rather disordered 3D close-packed structure at the bottom of the capillary. The dipolar and excluded volume interactions are responsible for the structure formation at the bottom part of the sediment whereas the upper part of the sediments is populated with the 2D structures because of the dipolar attraction between the nanoparticles. Our findings are in good agreement with theoretical results on the assembly of these particles. This study allows us to determine a colloidal phase diagram where one can manipulate the crystalline phase and the lattice parameters of the colloidal crystal by externally tuning stimuli such as the magnetic field and concentration gradient.

AUTHOR INFORMATION

Corresponding Author

*E-mail: malik@uwm.edu.

Notes

The authors declare no competing financial interest.

ACKNOWLEDGMENTS

V.M. thanks the Swiss National Science Foundation (SNF) for financial support (grant no. PBFRP2-134284). Y.Y. is grateful for financial support from the U.S. Army Research Laboratory (award no. W911NF-10-1-0484), the Research Corporation for Science Advancement (Cottrell Scholar Award), and a DuPont Young Professor Grant. M.S. is funded by the National Science Foundation (grants NSF-0952643 and NSF-1121770). We thank Dmyto Byelov, Anke Leferinkop Reinink, Esther van den Pol, and the personnel of beamline BM-26B for their help with the setup and synchrotron measurements. Beam time was kindly provided by the Nederlandse Organisatie voor Wetenschappelijk Onderzoek (NWO). Namrta Purwar is acknowledged for reading and commenting on the manuscript.

REFERENCES

(1) Ge, J.; Hu, Y.; Yin, Y. Highly tunable superparamagnetic colloidal photonic crystals. *Angew. Chem., Int. Ed.* **2007**, *46*, 7428−7432.

(2) Camargo, P. H. C.; Li, Z.-Y.; Xia, Y. Colloidal building blocks with potential for magnetically configurable photonic crystal. *Soft Matter* **2007**, *3*, 1215−1222.

(3) Butter, K.; Bomans, P. H. H.; Frederik, P. M.; Vroege, G. J.; Philipse, A. P. Direct observation of dipolar chains in iron ferrofluids by cryogenic electron microscopy. *Nat. Mater.* **2003**, *2*, 88−91.

(4) Yethiraj, A.; van Blaaderen, A. A colloidal model system with an interaction tunable from hard sphere to soft and dipolar. *Nature* **2003**, *421*, 513−517.

(5) Klokkenburg, M.; Vonk, C.; Claesson, E. M.; Meeldijk, J. D.; Erne, B. H.; Philipse, A. P. Direct imaging of zero-field dipolar structures in colloidal dispersions of synthetic magnetite. *J. Am. Chem. Soc.* **2004**, *51*, 16706−16707.

(6) Hynninen, A.-P.; Dijkstra, M. Phase diagram of dipolar hard and soft spheres: manipulation of colloidal crystal structures by an external field. *Phys. Rev. Lett.* **2005**, *94*, 138303.

(7) Klokkenburg, M.; Erne, B. H.; Meeldijk, J. D.; Widenmann, A.; Petukhov, A. V.; Dullens, R. P. A.; Philipse, A. P. In situ imaging of field-induced hexagonal columns in magnetite ferrofluids. *Phys. Rev. Lett.* **2006**, *97*, 185702.

(8) Agarwal, A. K.; Yethiraj, A. Low-density ordered phase in brownian dipolar colloidal suspensions. *Phys. Rev. Lett.* **2009**, *102*, 198301.

(9) Yoon, T. J.; Yu, K. N.; Kim, E.; Kim, J. S.; Kim, B. G.; Yun, S. H.; Sohn, B. H.; Cho, M. H.; Lee, J. K.; Park, S. B. Specific targeting, cell sorting, and bioimaging with smart magnetic silica core-shell nanomaterials. *Small* **2006**, *2*, 209−215.

(10) Lee, J.; Lee, Y.; Youn, J. K.; Na, H. B.; Yu, T.; Kim, H.; Lee, S. M.; Koo, Y. M.; Kwak, J. H.; Park, H. G.; Chang, H. N.; Hwang, M.; Park, J. G.; Kim, J.; Hyeon, T. Simple synthesis of functionalized superparamagnetic magnetite/silica core-shell nanoparticles and their application as magnetically separable high performance biocatalysts. *Small* **2008**, *4*, 143−152.

(11) Lee, J.-H.; Huh, Y.-M.; Jun, Y.-w.; Seo, J.-w.; Jang, J.-t.; Song, H.-T.; Kim, S.; Cho, E.-J.; Yoon, H.-G.; Suh, J.-S.; Cheon, J. Artificially engineered magnetic nanoparticles for ultra-sensitive molecular imaging. *Nat. Med.* **2007**, *13*, 95−99.

(12) Lee, J.-H.; Lee, K.; Moon, S. H.; Lee, Y.; Gwan Park, T.; Cheon, J. All-in-one target-cell-specific magnetic nanoparticles for simultaneous molecular imaging and siRNA delivery. *Angew. Chem., Int. Ed.* **2009**, *48*, 4174−4179.

(13) Xu, C.; Xu, K.; Gu, H.; Zhong, X.; Guo, Z.; Zheng, R.; Zhang, X.; Xu, B. Nitrilotriacetic acid modified magnetic nanoparticles as a general agent to bin histidine-tagged protein. *J. Am. Chem. Soc.* **2004**, *126*, 3392−3393.

(14) Lu, A.-H.; Salabas, E. L.; Schuth, F. Magnetic nanoparticles: synthesis, protection, functionalization, and application. *Angew. Chem., Int. Ed.* **2007**, *46*, 1222−1244.

(15) Zhao, X.; Tapec-Dytioco, R.; Wang, K.; Tan, W. Collection of trace amounts of DNA/mRNA molecules using geomagnetic nanocaptures. *Anal. Chem.* **2003**, *75*, 3476.

(16) Sonti, S. V.; Bose, A. DNA isolation using avidin coated magnetic nanoclusters. *Colloids Surf., B* **1997**, *8*, 199−204.

(17) Ge, J.; Hu, Y.; Biasini, M.; Beyermann, W. P.; Yin, Y. Superparamagnetic magnetite colloidal nanocrystal clusters. *Angew. Chem., Int. Ed.* **2007**, *46*, 4342−4345.

(18) Ge, J.; Yin, Y. Magnetically responsive colloidal photonic crystals. *J. Mater. Chem.* **2008**, *18*, 5041−5045.

(19) Ge, J.; Goebl, J.; He, L.; Lu, Z.; Yin, Y. Rewritable photonic papers with hygroscopic salt solution as ink. *Adv. Mater.* **2009**, *21*, 4259−4364.

(20) He, L.; Hu, Y.; Han, X.; Lu, Y.; Lu, Z.; Yin, Y. Assembly and photonic properties of superparamagnetic colloids in complex magnetic fields. *Langmuir* **2011**, *27*, 13444−13450.

(21) He, L.; Hu, Y.; Kim, H.; Ge, J.; Kwon, S.; Yin, Y. Magnetic assembly of non-magnetic particles into photonic crystal structure. *Nano Lett.* **2010**, *10*, 4708−4714.

(22) Ge, J.; Yin, Y. Magnetically tunable colloidal photonic structures in alkanol solution. *Adv. Mater.* **2008**, *20*, 3485−3491.

(23) Borsboom, M.; Bras, W.; Cerjak, I.; Detollenaere, D.; van Loon, D. G.; Goedtkindt, P.; Konijnenburg, M.; Lassing, P.; Levine, Y. K.; Munneke, B.; Oversluizen, M.; van Tol, R.; Vlieg, E. The Dutch-Belgian beamline at the ESRF. *J. Synchrotron Radiat.* **1998**, *5*, 518−520.

(24) Petukhov, A. V.; Thijssen, J. H. J.; Hart, D. C.; Imhof, A.; van Blaaderen, A.; Dolbnya, I. P.; Snigirev, A.; Moussaid, A.; Snigireva, I. Microradian X-ray diffraction in colloidal photonic crystal. *J. Appl. Crystallogr.* **2006**, *39*, 137−144.

(25) Thijssen, J. H. J.; Petukhov, A. V.; 't Hart, D. C.; Imhof, A.; van der Werf, C. H. M.; Schropp, R. E. I.; van Blaaderen, A. Characterization of photonic colloidal single crystals by Microradian X-ray diffraction. *Adv. Mater.* **2006**, *18*, 1662−1666.

(26) Heinrich, D.; Goni, A. R.; Smessaert, A.; Klapp, S. H. L.; Cerioni, L. M. C.; Osan, T. M.; Pusiol, D. J.; Thomsen, C. Dynamics of field induced formation of hexagonal zipped-chain superstructures in magnetic colloids. *Phys. Rev. Lett.* **2011**, *106*, 208301.

(27) Klokkenburg, M.; Erné, B.; Wiedenmann, A.; Petukhov, A. V.; Philipse, A. P. Dipolar structures in magnetite ferrofluids studied with

small angle neutron scattering with and without applied magnetic field. *Phys. Rev. E* **2007**, *75*, 051408.
(28) Goyal, A.; Hall, C. K.; Velev, O. D. Bicontinous gels formed by self-assembly of dipolar colloid particles. *Soft Matter* **2010**, *6*, 480−484.
(29) Goyal, A.; Hall, C. K.; Velev, O. D. Phase diagram of stimuli responsive materials containing dipolar colloidal particles. *Phy. Rev. E* **2008**, *77*, 031401.
(30) Schmidle, H.; Hall, C. K.; Velev, O. D.; Klapp, S.H. L. Phase diagram of two dimensional systems of dipole like colloids. *Soft Matter* **2012**, *8*, 1521−1531.

■ NOTE ADDED AFTER ASAP PUBLICATION

This article was published ASAP on July 25, 2012. Equation 1 has been modified. The correct version was published on August 29, 2012.